


# Distinct binding kinetics of E-, P- and L-selectins to CD44

Linda Li<sup>1,2</sup>, Qihan Ding<sup>2,3</sup>, Jin Zhou<sup>2,3</sup>, Yi Wu<sup>2,3</sup>, Mingkun Zhang<sup>2,3</sup>, Xingming Guo<sup>1</sup>, Mian Long<sup>2,3</sup> and Shouqin Lü<sup>2,3</sup> 

1 Key Laboratory of Biorheology Science and Technology, Ministry of Education, College of Bioengineering, Chongqing University, Chongqing, China

2 Center of Biomechanics and Bioengineering, Key Laboratory of Microgravity (National Microgravity Laboratory), Beijing Key Laboratory of Engineered Construction and Mechanobiology, and CAS Center for Excellence in Complex System Mechanics, Institute of Mechanics, Chinese Academy of Sciences, Beijing, China

3 School of Engineering Science, University of Chinese Academy of Sciences, Beijing, China

## Keywords

binding epitope; binding kinetics; CD44; selectin

## Correspondence

X. Guo, Key Laboratory of Biorheology Science and Technology, Ministry of Education, College of Bioengineering, Chongqing University, Chongqing 400044, China

Tel: +86-023-65112676

E-mail: guoxm@cqu.edu.cn

Or

M. Long and S. Lü, Center of Biomechanics and Bioengineering, Key Laboratory of Microgravity (National Microgravity Laboratory), Beijing Key Laboratory of Engineered Construction and Mechanobiology, and CAS Center for Excellence in Complex System Mechanics, Institute of Mechanics, Chinese Academy of Sciences, Beijing 100190, China

Tel: +86-010-82544131

E-mails: mlong@imech.ac.cn (ML);

lsq@imech.ac.cn (SL)

Molecular-level selectin-cluster of differentiation 44 (CD44) interactions are far from clear because of the complexity and diversity of CD44 glycosylation and isoforms expressed on various types of cells. By combining experimental measurements and simulation predictions, the binding kinetics of three selectin members to the recombinant CD44 were quantified and the corresponding microstructural mechanisms were explored, respectively. Experimental results showed that the E-selectin-CD44 interactions mainly mediated the firm adhesion of microbeads under shear flow with the strongest rupture force. P- and L-selectins had similar interaction strength but different association and dissociation rates by mediating stable rolling and transient adhesions of microbeads, respectively. Molecular docking and molecular dynamics (MD) simulations predicted that the binding epitopes of CD44 to selectins are all located at the side face of each selectin, although the interfaces denoted as the hinge region are between lectin and epidermal growth factor domains of E-selectin, Lectin domain side of P-selectin and epidermal growth factor domain side of L-selectin, respectively. The lowest binding free energy, the largest rupture force and the longest lifetime for E-selectin, as well as the comparable values for P- and L-selectins, demonstrated in both equilibration and steered MD simulations, supported the above experimental results. These results offer basic data for understanding the functional differences of selectin-CD44 interactions.

Linda Li and Qihan Ding contributed equally to this work.

(Received 17 July 2021, revised 22 October 2021, accepted 26 November 2021)

doi:10.1111/febs.16303

## Abbreviations

AFM, atomic force microscope; CD44, cluster of differentiation 44; CR, consensus repeats; DFS, dynamic force spectroscopy; DPBS, Dulbecco's phosphate-buffered saline; EGF, epidermal growth factor; HABD, hyaluronic acid binding domain; PSGL-1, P-selectin glycoprotein ligand-1; SMD, steered molecular dynamics.

## Introduction

The interactions between selectins and their glycoconjugate ligands play key roles in mediating blood cell tethering to and rolling on endothelial cells with respect to triggering the signaling cascade leading to leukocyte recruitment for sites of inflammation and injury [1]. The selectins have three members: P-, E- and L-selectins. All of them consist of an N-terminal C-type lectin domain, an epidermal growth factor (EGF)-like module, multiple copies of consensus repeats (CRs; two, six and nine CRs for L-, E- and P-selectin, respectively), a transmembrane segment and a short cytoplasmic domain [1]. P-selectin glycoprotein ligand-1 (PSGL-1), expressed at the top of leukocyte microvilli, is one of well characterized glycoconjugate ligands of selectins. Selectin–PSGL-1 interactions are extensively investigated including steric or dynamic microstructural features at the atomic level [2–7], intrinsic binding kinetics [8–10] and external force regulations at the molecular level [11–16], as well as intracellular signaling at the cellular level [17–19]. The minimum functional unit of selectin–PSGL-1 interactions includes the lectin and EGF domains of the selectin side and specific N-terminal sulfoglycopeptide of the PSGL-1 side, and the binding sites located at the calcium ion and nearby residues of selectin lectin domain. Intrinsic rapid association and dissociation rates of selectin–PSGL-1 interactions guarantee their function of modulating the instantaneous capture of blood cells from the blood flow and balancing rapid rolling. Extrinsic physical factors such as an external force could regulate the kinetics of selectin–PSGL-1 interactions, and corresponding microstructural explanations mainly include force-regulated allostery of selectin lectin and EGF domains or force-induced sliding-rebinding mode of the selectin–PSGL-1 complex.

Cluster of differentiation 44 (CD44) is another important glycoconjugate ligand of selectins with respect to mediating leukocyte extravasation during inflammation, as well as inducing adhesions between tumor cells and blood cells or endothelial cells [20]. Different isoforms of CD44 expressing on various cells have distinct binding affinities for selectins. Variant isoforms of CD44 (CD44v) on LS174T colon carcinoma cells possess binding activity to all three selectin members, although the standard isoform of CD44 (CD44s) on hematopoietic-progenitor cells is primarily an ligand of only E- and L-selectins, and CD44s on HL-60 only bind to E- and P-selectins effectively [21,22]. CD44 is also a major E-selectin ligand on human activated T-cells or neutrophils [20,23]. Thus, E-selectin is an intrinsic receptor for extensive CD44 isoforms but P- and L-selectins are selective

to specific CD44 isoforms. In terms of biological function, the ligands of PSGL-1 and CD44 take on different roles by binding to E-selectin. The former plays a major role in the initial leukocyte capture, whereas the latter controls corresponding rolling velocity by mediating E-selectin-dependent redistribution of PSGL-1 and L-selectin [20]. Meanwhile, both CD44 and PSGL-1 share a common signaling pathway to induce  $\alpha_L\beta_2$  integrin-mediated slow leukocyte rolling through binding to E-selectin [17]. Comparatively, the molecular mechanism of selectin–CD44 interactions is far from clear compared to that of selectin–PSGL-1 interactions. On the one hand, quantification of selectin–CD44 interactions at the molecular level, especially for binding kinetics and strength under two-dimensional conditions mimicking the physiological environment, are still not systematic. Although sporadic comparisons of three-dimensional binding kinetics between E-selectin–PSGL-1 and E-selectin–CD44 systems are performed based on surface plasmon resonance technology [24–26], the binding strength of P-selectin–CD44v is quantified using an atomic force microscope (AFM) assay [27], and primary dependences of LS174T CD44-mediated adhesion to three types of selectin-coated substrates on a range of shear stresses are quantified using a flow chamber assay [21]. The systematic measurements of binding kinetics and strength under two-dimensional conditions, as well as difference comparisons among the three selectin–CD44 interaction systems, are still needed for elucidating corresponding biological functions.

On the other hand, the microstructural features of selectin–CD44 interactions are still lacking. It is well known that the ligand of PSGL-1 binds to the head face of the selectin lectin domain, which is almost perpendicular to the axis linking the centers of the lectin and EGF domains, and the specific interactions between selectin and PSGL-1 are mainly contributed to by the interactions of calcium ion and nearby residues located in the head face of the lectin domain [2]. The microstructural features of N-terminal hyaluronic acid binding domain (HABD) domain of CD44, which is also known as the main binding site of other CD44 counterparts such as collagen, laminin, fibronectin, and selectin [28], and the complex features of HABD–HA interactions are well characterized based on structural biological techniques [29–31] and molecular simulations [32]. However, the interacting features between selectin and CD44 at atomic level are still not clear.

In the present study, the binding kinetics and mechanical strength of three selectin–CD44 binding systems were compared using both parallel plate flow chamber and AFM assays under the same experimental conditions and with the same ligand of

recombinant CD44. Corresponding microstructural features were first predicted using molecular docking, then equilibration molecular dynamics simulations and steered molecular dynamics (SMD) simulations were performed to investigate the contributions of key binding sites to mechanical strength. The results obtained provide an insight into understanding the structure–function relationship of selectin–CD44 interactions, as well as differences among the three selectin members for binding to the common ligand of CD44.

## Results

### Selectin–CD44 interactions mediated distinct microbead adhesions under shear flow

It is well known that selectin–CD44 interactions mediate cell–cell adhesions under blood flow in

physiological or pathological environments. To investigate differences for the three selectin members with respect to binding to CD44, a flow chamber assay was used first to quantify their capabilities of mediating microbead adhesions under shear flow that mimicked *in vivo* cellular adhesions under blood flow (Fig. S1A, B). The results showed that E-/P-/L-selectin–CD44 interactions mediated distinct microbead adhesion dynamics and strengths based on the comparable microbead coating densities (Fig. S1C, D). Although most microbeads were stably adhered to the substrate with instantaneous velocities around zero and unchanged displacements by E-selectin–CD44 interactions under shear stress of  $0.5 \text{ dyne}\cdot\text{cm}^{-2}$  (Fig. 1A and Fig. S2B, Video S1), P-selectin–CD44 interactions mediated two phases of adhesion dynamics: one was stable rolling of most microbeads with slowly and linearly increased displacements and jagged instantaneous

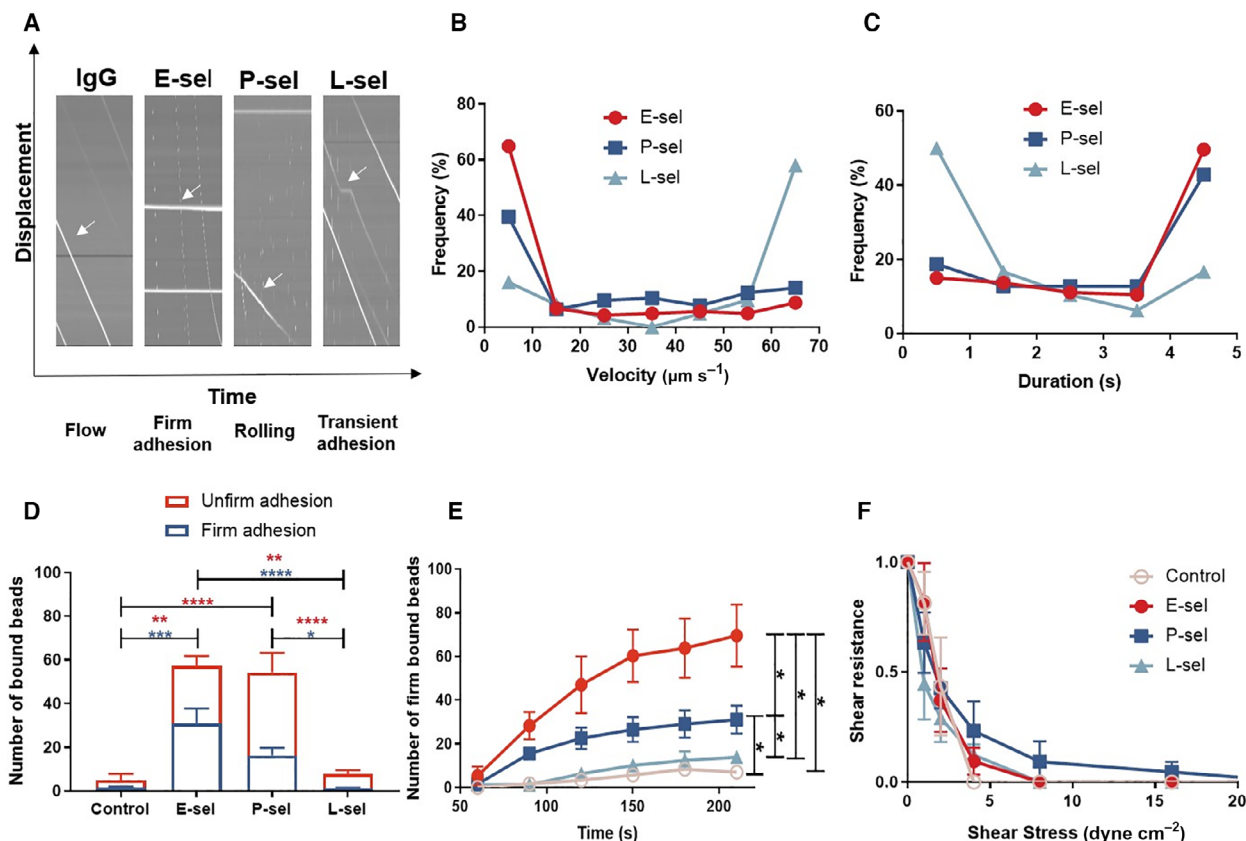


**Fig. 1.** Differences in microbead adhesion dynamics mediated by E-/P-/L-selectin–CD44 interactions under shear stress of  $0.5 \text{ dyne}\cdot\text{cm}^{-2}$  by flow chamber tests. (A) Typical trajectories of adhered microbeads mediated by non-specific IgG–CD44 and specific E-/P-/L-selectin–CD44 interactions. Distributions of average velocity (B) and duration (C) of adhered microbeads, and numbers of firmly or unfirmly adhered microbeads (D) at the moment of 90 s. (E) Numbers of firmly adhered microbeads in a 210-s time-lapsed course. (F) Evolutions of firmly adhered microbeads in a stress-dependent course. Data are shown as the mean  $\pm$  SE of at least three independent repeats. Two-way ANOVA tests were performed for the data. \* $P < 0.05$ , \*\* $P < 0.01$ , \*\*\* $P < 0.001$ , \*\*\*\* $P < 0.0001$ .

velocities, and the other was similar stable adhesions of a small number of microbeads to those mediated by E-selectin–CD44 interactions (Fig. 1A and Fig. S2C, Video S2). L-selectin–CD44 interactions mediated tethering adhesions of microbeads with short-lived stopping (Fig. 1A and Fig. S2D, Video S3). Comparatively, most of the control microbeads flowed away along the shear flow with stable instantaneous velocities and steep and linear increases of displacement (Fig. 1A and Fig. S2A, Video S4). Distributions of average velocity and adhesion duration based on both firmly and unfirmly adhered microbeads of a 5-s time window around the moment of 90 s in a 210-s time-lapsed binding course demonstrated similar trends. Stable adhesions of most microbeads mediated by E-selectin–CD44 interactions resulted in the smallest average velocities with the highest frequency in the region of 0–10  $\mu\text{m}\cdot\text{s}^{-1}$ . L-selectin–CD44 interactions mediated short-lived tethering resulting in the largest average velocities with the highest frequency in the region of 60–70  $\mu\text{m}\cdot\text{s}^{-1}$ . P-selectin–CD44 interactions mediated both rolling and firm adhesions that exhibited intermediate distributions between E- and L-selectins (Fig. 1B). The distributions of adhesion duration showed reverse trends compared to those of average velocity (Fig. 1C).

Besides adhesion dynamics, total adhesion numbers of microbeads also exhibited differences among the three selectin members. Both firmly and unfirmly adhered numbers of microbeads of a 5-s time window around the moment of 90 s mediated by E-selectin–CD44 or P-selectin–CD44 interactions were significantly higher compared to those for L-selectin–CD44 interactions. E-selectin and P-selectin did not yield evident differences, although the ratio of unfirm adhesion number for P-selectin was slightly higher compared to those of E-selectin, consistent with the above dynamic features where P-selectin–CD44 mainly mediated rolling adhesion. In addition, even though L-selectin–CD44 interactions mediated specific tethering adhesion, corresponding adhesion numbers were comparable with those of the control case (Fig. 1D). The number of evolutions of only firm adhesion microbeads in the 210-s time-lapsed course showed similar trends. The microbead number of firm adhesion mediated by the E-selectin–CD44 interaction increased quickly with time and reached the highest value. Those for the P-selectin–CD44 interaction achieved middle values and those for L-selectin–CD44 were comparable to the control case (Fig. 1E). By contrast, the shear resistance did not show a significant difference among the three members with slightly higher values for P-selectin (Fig. 1F). The above results for both adhesion dynamics and capabilities indicated that, for the

common ligand of CD44, the three selectin members have distinct interactions with the strongest binding capability for E-selectin, the weakest ability for L-selectin and an intermediate ability for P-selectin.

Dependences of selectin–CD44 interactions on shear stress were also quantified by comparing their variation under typical shear stresses of 0.5 and 1.5  $\text{dyne}\cdot\text{cm}^{-2}$ . Although high shear stress significantly decreased numbers of adhered microbeads in the entire 210-s course for both E- and P-selectins, L-selectin showed contrary behaviors with a significant increase of adhered microbead number under high shear stress of 1.5  $\text{dyne}\cdot\text{cm}^{-2}$  (Fig. 2A,D,G). Shear resistance did not show obvious variation for all of them, except for a slight decrease in P-selectin (Fig. 2B,E,H). The contrary effects of shear stress on these three selectin members from 0.5 to 1.5  $\text{dyne}\cdot\text{cm}^{-2}$  smoothed their differences, resulting in comparable values for both binding and shear resistance under 1.5  $\text{dyne}\cdot\text{cm}^{-2}$  (Fig. 2C,F,I, and Fig. S3). These results indicated that selectin–CD44 interactions were modulated by external forces, and the increase of shear stress from 0.5 to 1.5  $\text{dyne}\cdot\text{cm}^{-2}$  decreased the bindings of E- or P-selectin–CD44 interactions but enhanced that of the L-selectin–CD44 system.

### Selectin–CD44 interactions presented distinct mechanical strength and binding kinetics

The above results from the flow chamber test indicated the distinct binding of selectins to the common ligand of CD44 by an indirect index of microbead adhesion. To test this further, an AFM assay was further performed for direct measurements of the mechanical strengths of selectin–CD44 and corresponding binding kinetics were also predicted based on dynamic force spectroscopy (DFS) theory (Fig. S4A,B). The specific bindings of each selectin–CD44 system were represented by their significantly higher adhesion frequency compared to that of control case under contact duration of 50 or 500 ms (Fig. S4C,D). In addition, the systemic spring constant  $k$ , defined as the spring constant of the selectin–CD44 complex in series with that of the cantilever, was different among the three members (Fig. 3A–F). The L-selectin–CD44 system had the highest  $k$  and that of the P-selectin–CD44 system was the lowest (Fig. 3G,H), which was reasonable because L-selectin has the shortest length, with only two CR domains, and P-selectin is the longest, with nine CR domains, and E-selectin stays in middle, with six CR domains. The combination of adhesion frequency and systemic spring constant tests validated the reliability of the AFM assay for the measurement of selectin–CD44 interactions.

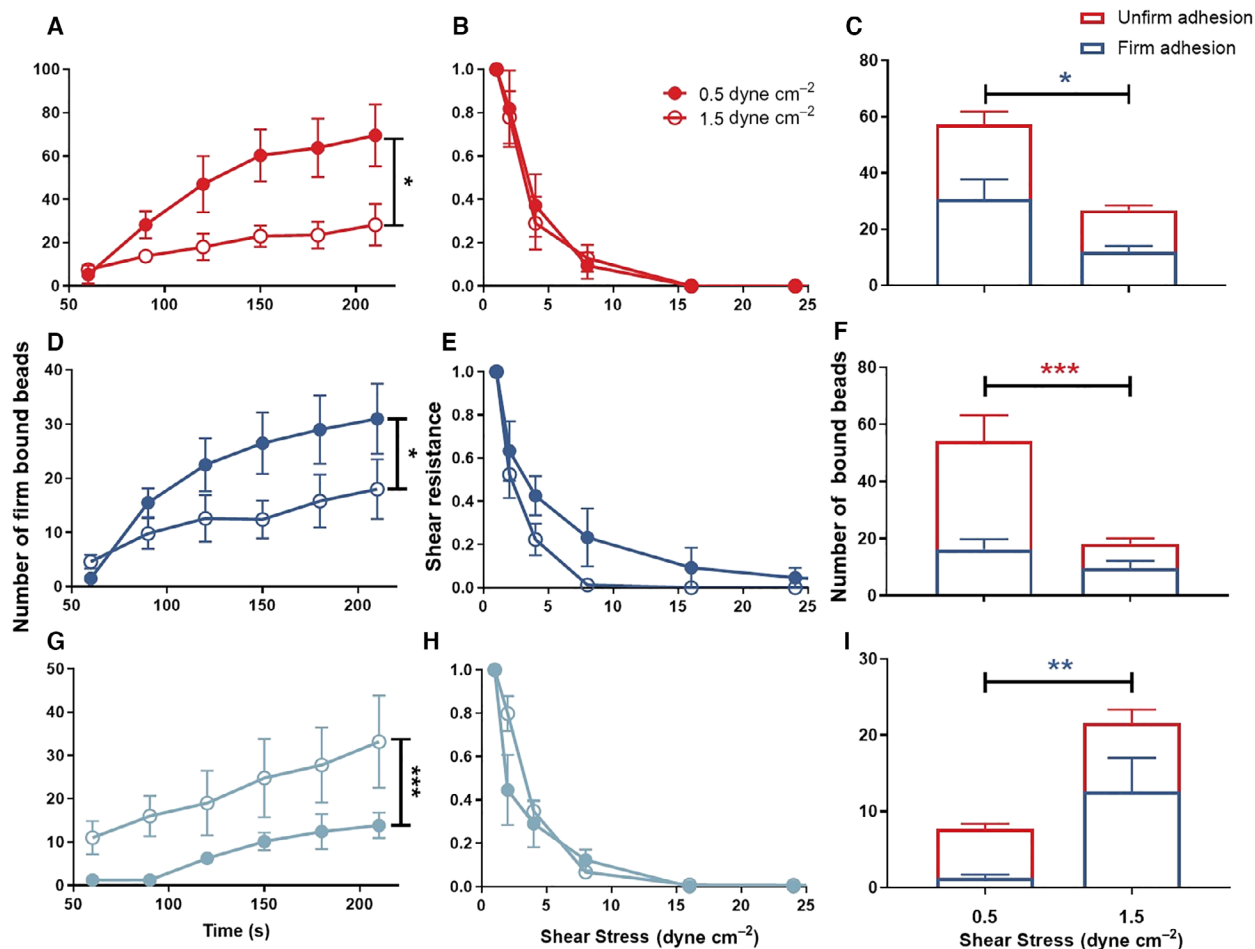


**Fig. 2.** Shear stress dependence on microbead adhesions mediated by E-/P-/L-selectin-CD44 interactions. Showing the numbers of firmly adhered microbeads in a time-lapsed course (A, D, G) or a stress-dependent manner (B, E, H) and of both unfirmly and firmly adhered microbeads at the moment of 90 s in a time-lapse course (C, F, I), which were mediated by E-selectin- (A-C), P-selectin- (D-F) and L-selectin-CD44 (G-I) interactions, respectively. Data are shown as the mean  $\pm$  SE of at least three independent repeats. \* $P < 0.05$ , \*\* $P < 0.01$ , \*\*\* $P < 0.001$ .

The dependences of selectin-CD44 mechanical strength on retract velocity were then compared among the three selectin members. The results showed that all rupture forces increased first and then reached a plateau following the increase of retract velocity (Fig. 4A-H), although those from the control case did not present similar trends (Fig. S4E,F). Specifically, the E-selectin-CD44 system presented the highest rupture forces based on both contact times of 50 and 500 ms. The rupture forces of the L-selectin-CD44 system were slightly higher than those of the P-selectin-CD44 system for a contact time of 50 ms, whereas data from the two systems became comparable for a contact time of 500 ms. A long contact time of 500 ms increased the rupture forces compared to those of 50 ms for all three selectin-CD44 systems, especially

for the two systems of E- and P-selectins, but less so for L-selectin-CD44 (Fig. 4D,H). These results indicated that, on the one hand, E-selectin-CD44 interactions have the strongest interactions compared to the P- and L-selectin-CD44 interactions and, on the other hand, L-selectin-CD44 interactions present the fastest association compared to the other two systems, with the rupture forces for both 50 and 500 ms being comparable. These data were also consistent with those obtained from the flow chamber assay: E-selectin-CD44 interactions mainly mediated the firm adhesion of microbeads and L-selectin-CD44 interactions could still effectively mediate microbead adhesion under the higher shear stress of  $1.5 \text{ dyne cm}^{-2}$ .

Dissociation kinetics could also be predicted based on DFS theory. The zero-force dissociation rate  $k_r^0$

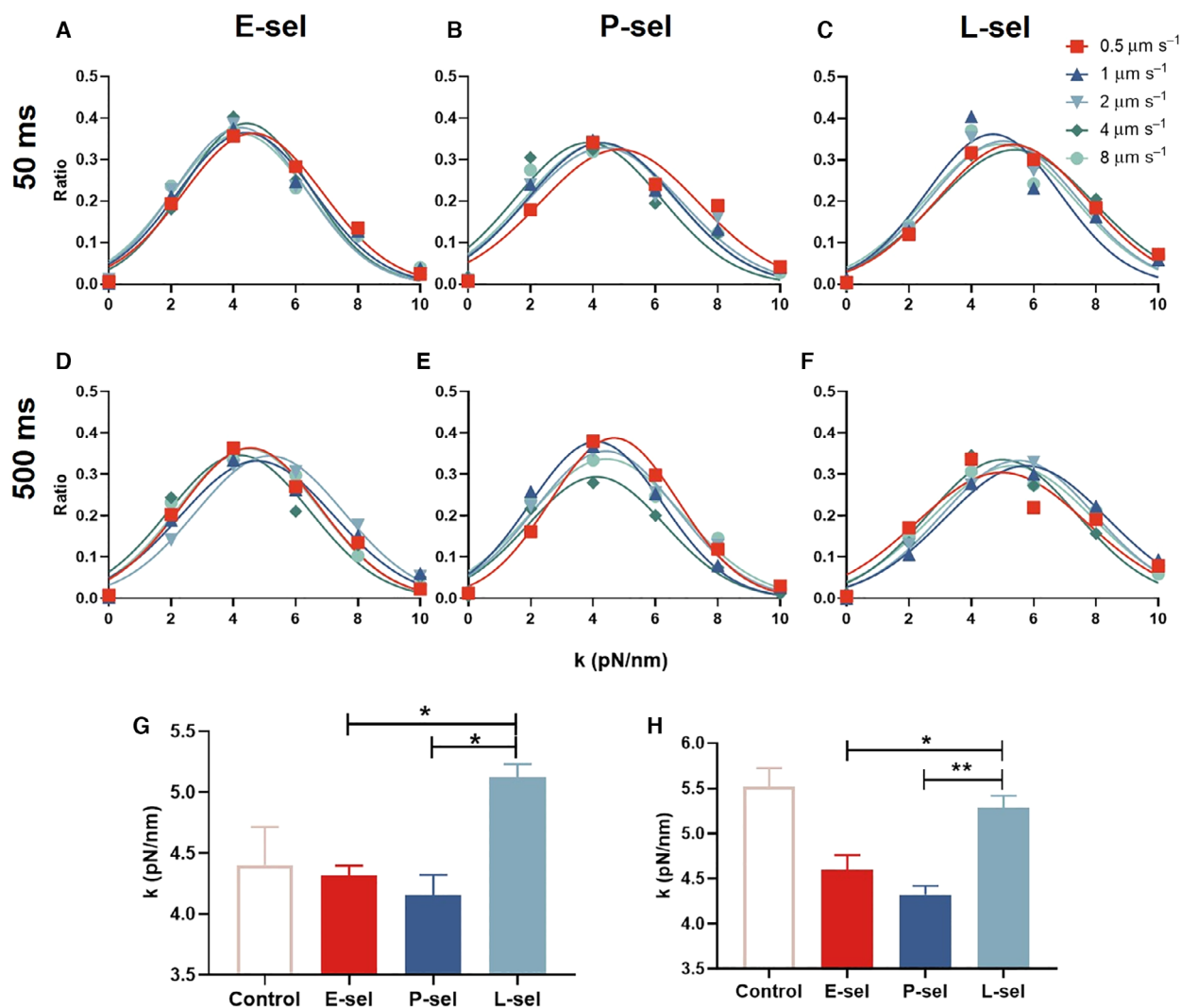


**Fig. 3.** Spring constant  $k$  of E-/P-/L-selectin-CD44 pairs by AFM tests. Spring constant distributions of E-selectin- (A, D), P-selectin- (B, E) and L-selectin-CD44 (C, F) complexes upon retract velocities are shown based on contact times of 50 (A–C) or 500 ms (D–F). Gaussian fitting lines were also presented for each distribution. Averages of Gaussian fitting medians of all retract velocities for each selectin-CD44 pair are presented in (G) and (H) for a contact time of 50 (G) and 500 ms (H). Here, the controls are directly presented as the mean  $\pm$  SE of all raw data. The approach velocity was set as  $1 \mu\text{m s}^{-1}$  for all measurements, and data for each case are from at least three independent repeats. \* $P < 0.05$ , \*\* $P < 0.01$ .

and the width of the energy well  $a$  were obtained by fitting the data of rupture forces on loading rate (Fig. 4I–K). Here, the loading rate was defined as the product of the retract velocity and the systemic spring constant, the latter of which was estimated from the data shown in Fig. 3. The results indicated that  $k_r^0$  decreased gradually from the E-selectin-CD44 system to the P-selectin-CD44 and to L-selectin-CD44 systems for contact times of both 50 and 500 ms, and the long contact time of 500 ms resulted in a significant increase of  $k_r^0$  for all three selectin-CD44 interactions

(Fig. 4L). The width of the energy well  $a$  of P-selectin-CD44 interactions was the largest and that of E-selectin-CD44 interactions was the smallest for a contact time of 50 ms, even though the three systems did not show a distinct difference. Extension of contact time from 50 to 500 ms decreased the width of the energy well  $a$  for all three systems, with gradually increased values from E-selectin-CD44 to the P-selectin-CD44 and to L-selectin-CD44 systems (Fig. 4M). One idealized case occurring in the strongest E-selectin-CD44 interactions, as exhibited via flow

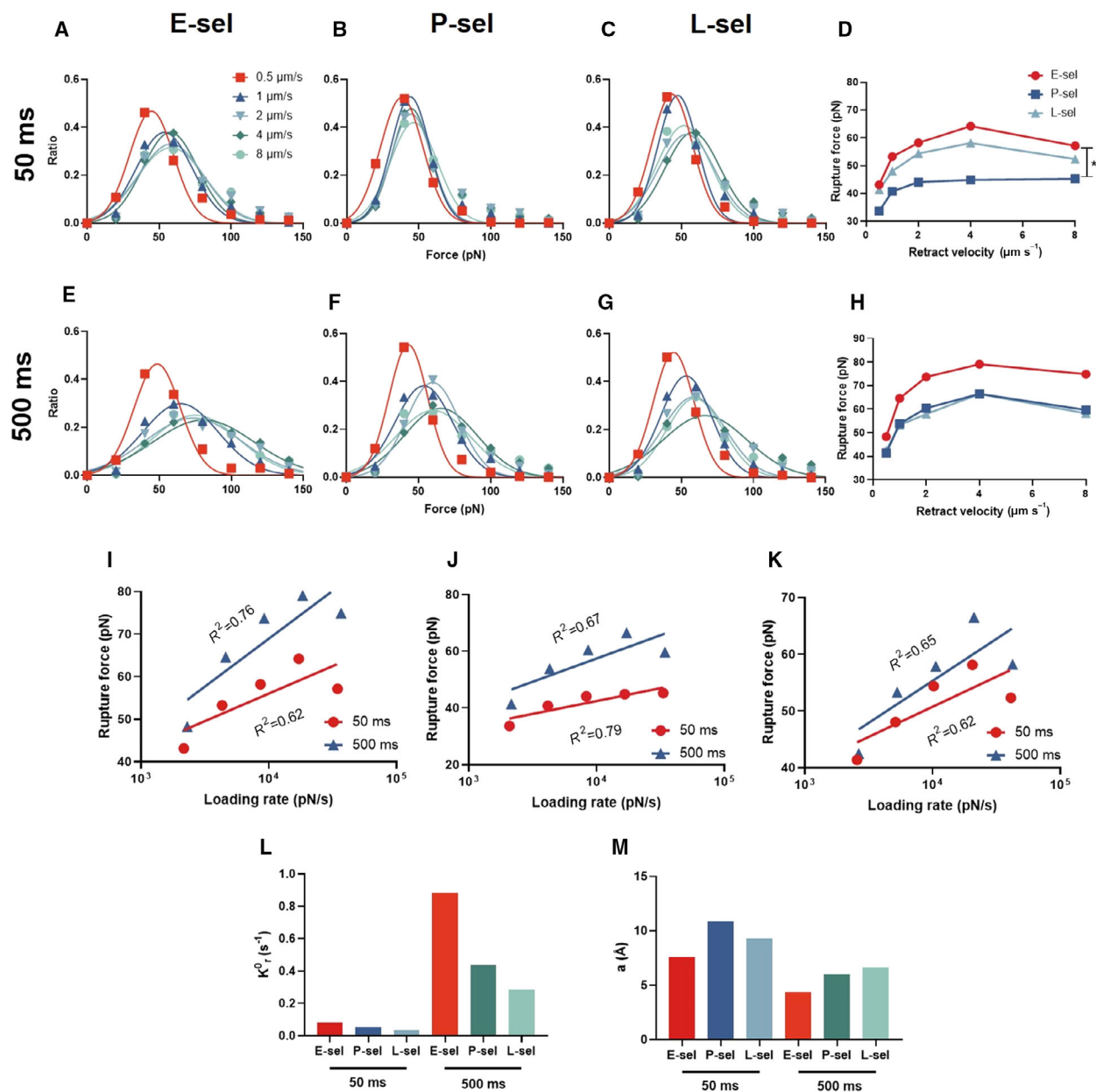


**Fig. 4.** Rupture forces and binding kinetics of E-/P-/L-selectin-CD44 interactions. (A–H) Dependence of rupture force on the retract velocity for a contact time of 50 (A–D) or 500 ms (E–G) are presented with the respective Gaussian fitting lines for E-selectin- (A, E), P-selectin- (B, F) and L-selectin-CD44 (C, G) interactions. Corresponding medians of Gaussian fittings for a contact time of 50 and 500 ms are shown in (D) and (H), respectively. (I–K) Gaussian fitting medians of rupture force on loading rate are exhibited with the corresponding fitting lines based upon DFS theory for E-selectin- (I), P-selectin- (J) and L-selectin-CD44 (K) systems. Fitted binding kinetics of the dissociation rate  $k_r^0$  and the width of the energy well  $a$  are shown in (L) and (M), respectively. The approach velocity was set as  $1 \mu\text{m}\cdot\text{s}^{-1}$  for all experiments, and data for each case ARE from at least three independent repeats. Statistical tests were performed for (D) and (H) using Student's  $t$ -test, based on the Gaussian fitted median  $\pm$  confidence interval of all data. \* $P < 0.05$ .

chamber and AFM assays, had the smallest  $k_r^0$  and the narrowest width of energy well. However, the binding kinetics based on DFS theory showed contrary results. This inconsistency may indicate the sensitivity of selectin-CD44 interactions to an external force.

### Selectin-CD44 interactions presented distinct interaction patterns

The capabilities of selectin-CD44 interactions to mediate microbead adhesions and corresponding mechanical

strengths were both determined by their intrinsic microstructures. Although the structural features of selectin–PSGL-1 interactions have been investigated extensively, those of selectin–CD44 interactions are still lacking. Here, both molecular docking and MD simulations were further performed for elucidating the corresponding structural bases of selectin–CD44 interactions upon lectin and EGF domains of selectin and the HABD domain of CD44. The results indicated that the docking free energy of L-selectin–CD44 interaction candidates was the lowest and that of E-selectin–CD44 interactions yielded intermediate values (Fig. S5A). Analysis of the main binding sites involved in hydrogen bond forming for both CD44 and selectin sides showed the binding interface of L-selectin–CD44 interactions to be located in the N-terminal of the CD44 side and the EGF domain of the selectin side with extensive distributions of binding sites. The binding sites of E-selectin–CD44 docking mainly presented on the hydrogen bond between C77 of the CD44 side and N138 of the E-selectin side, located in the hinge region between the lectin and EGF domains. By contrast, P-selectin–CD44 docking candidates did not show any specific hydrogen bonds (Fig. S5B,C). These docking results implied that these three selectin members have different binding site distributions compared to the common ligand of CD44.

Molecular dynamics simulations were further performed based on the optimized docking candidates of the respective selectin–CD44 complex. Binding free energy was also calculated for the last 20-ns trajectories of each equilibration run. The results showed that the E-selectin–CD44 complex had the lowest energy of  $-23.67 \text{ kcal}\cdot\text{mol}^{-1}$ , and the energies of the P-selectin–CD44 and L-selectin–CD44 complexes were  $-12.02$  and  $-13.09 \text{ kcal}\cdot\text{mol}^{-1}$ , respectively (Fig. 5A–C). Although the binding interface analysis presented interaction profiles similar to those of docking, such that CD44 bound to the hinge region of E-selectin, to the Lectin domain of P-selectin and to the EGF domain of L-selectin, the specific binding sites were significantly altered upon the conformational relaxations in MD simulations compared to those from molecular docking. The prominent hydrogen bond interaction between E-selectin-N138 and CD44-C77 observed in docking candidates was replaced by the interaction between E-selectin-E33 and CD44-R41 for the E-selectin–CD44 interactions predicted from the MD simulations. Three residue pairs of P-selectin-Y5 and CD44-A20, P-selectin-K40 and CD44-D51, and P-selectin-K96 and CD44-D51 were found to play key roles in the P-selectin–CD44 interactions, instead of the almost non-specific interactions shown in docking. The extensive binding interface of the L-

selectin–CD44 complex exhibited in docking candidates was replaced by the key residue pairs of L-selectin-N139 and CD44-D23, L-selectin-T141 and CD44-N149, and L-selectin-V156 and CD44-R90 in MD simulations (Fig. 5D–F). These differences between the molecular docking and MD simulations resulted from the fact that the free relaxation of MD simulations allowed further optimization of the local conformation based on the initial docking complexes.

Binding free energy analysis of selectin–CD44 complexes in equilibration MD simulations showed that the E-selectin–CD44 complex had the strongest interaction, and those of the other two selectin–CD44 complexes were comparable. To verify these observations, *cv*-SMD simulations were further performed for all three complexes. The results indicated that the E-selectin–CD44 complex presented the largest rupture force and the longest lifetime. The P-selectin–CD44 and L-selectin–CD44 complexes did not show an obvious difference (Fig. 6A,B). Thus, the consistency between the SMD and equilibration results verified the strongest interactions of E-selectin–CD44 compared to the other two selectins. Typical force–time profiles and corresponding conformations of specific time points showed that the peak forces mainly resulted from the breakages of key residue pairs exhibited in equilibrations (Fig. 6C–E). Taken together, both molecular docking and MD simulations offered microstructural features for elucidating the interaction differences among the three selectin–CD44 complexes at the atomic level.

### Selectin–CD44 binding sites were different from those of the selectin–PSGL-1 interactions

It is well known that selectin–PSGL-1 interactions mediate the rolling of neutrophils under blood flow through PSGL-1 binding to the head face of the selectin lectin domain, which is approximately perpendicular to the axis linking the lectin and EGF domains, and these interactions are determined by calcium ion located at the binding interface. In the present study, the leaping features of instantaneous velocity also verified that the interactions of E-selectin (Fig. S6A), P-selectin (Fig. S6B) and L-selectin (Fig. S6C) binding to PSGL-1 mediated the rolling of microbeads. The above docking results for selectin–CD44 interactions, however, indicated that CD44 could bind to the side of the lectin–EGF axis of selectins, implying that the binding sites of CD44 and PSGL-1 are different for each selectin. Thus, respective blocking antibodies for selectin–PSGL-1 interactions were used to test the hypothesis that these antibodies could be invalid for selectin–CD44 interactions because CD44 presents



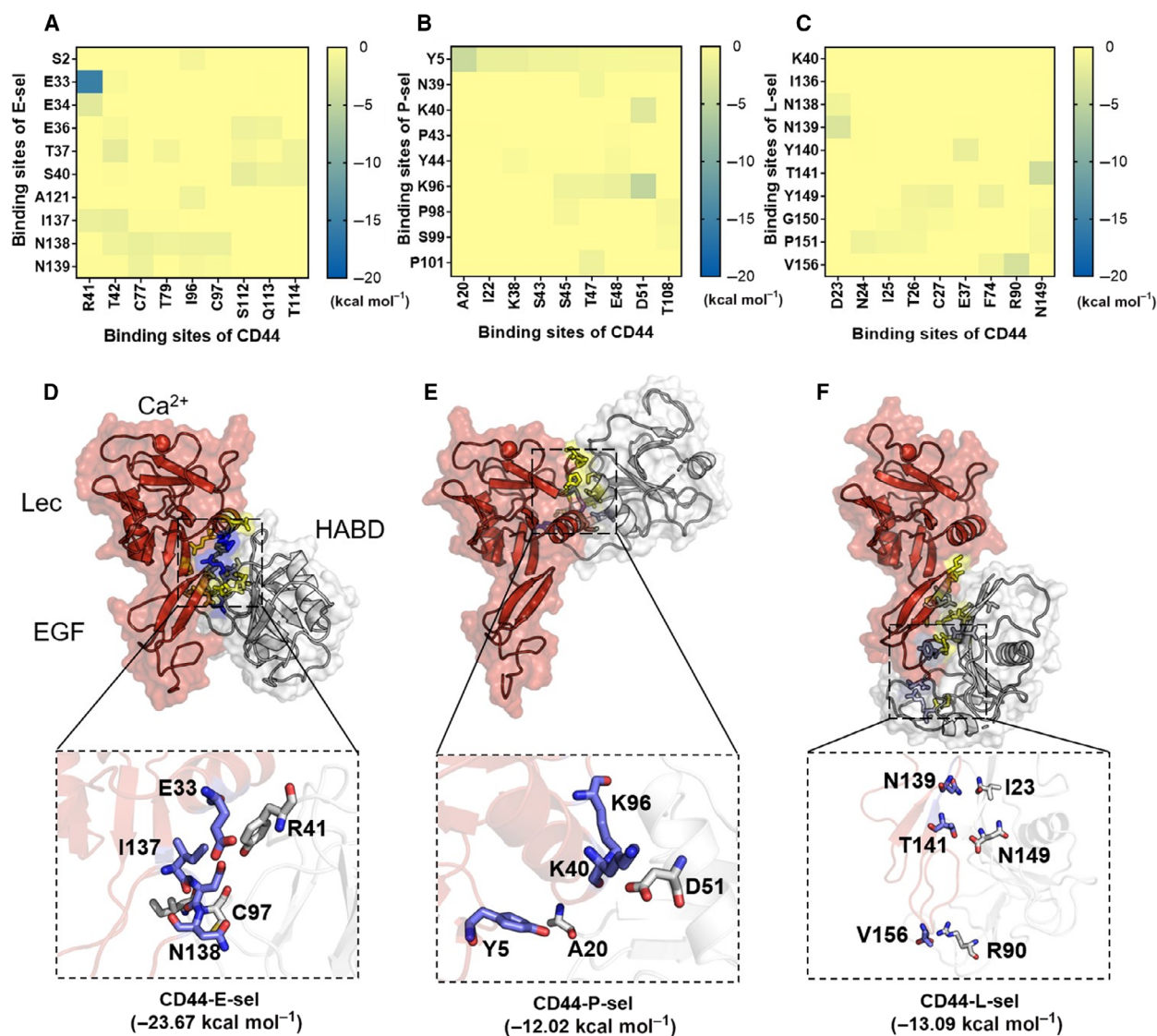


**Fig. 5.** Comparisons of binding sites among E-/P-/L-selectin–CD44 pairs from free MD simulations. (A–C) Distributions of pairwise free energy for E-selectin- (A), P-selectin- (B) and L-selectin–CD44 (C) pairs. Data are presented as the mean of the last 20-ns equilibration processes from two independent 50-ns equilibration simulation runs. (D–F) Typical complex conformations for E-selectin- (D), P-selectin- (E) and L-selectin–CD44 (F) pairs with selectins in red and CD44 in white. The binding surfaces were colored upon corresponding pairwise free energy bars of (A) to (C) and the main residues of both selectin and CD44 sides contributed to interaction free energy are indicated in zoom-in dotted-line boxes. Only the lectin and EGF domains of selectin and the HABD domain of CD44 were used for simulations in the present study.

different binding sites with PSGL-1. Our results showed that, although these three antibodies of ES-1 (Fig. 7A), G1 (Fig. 7B) and DREG56 (Fig. 7C) could effectively block the respective selectin–PSGL-1 interactions, only G1 was effective for blocking P-selectin–CD44 interactions. This exception appeared reasonable because the binding interface of CD44 to P-selectin is located at the side of the lectin domain, which is close to the binding interface of PSGL-1 (Fig. 5) and therefore efficient blocking of P-selectin–CD44 interactions

by G1 for P-selectin–PSGL-1 interactions may result from steric hindrance but not realistic space occupying. It should be noted that the coating densities of CD44 and PSGL-1 on microbeads were not comparable for the microbead adhesion measurements of the three selectins.

The key role of calcium ion for selectin–PSGL-1 interactions was also tested for selectin–CD44 interactions. The results showed that calcium ion was dispensable for both E- and P-selectin–CD44 interactions

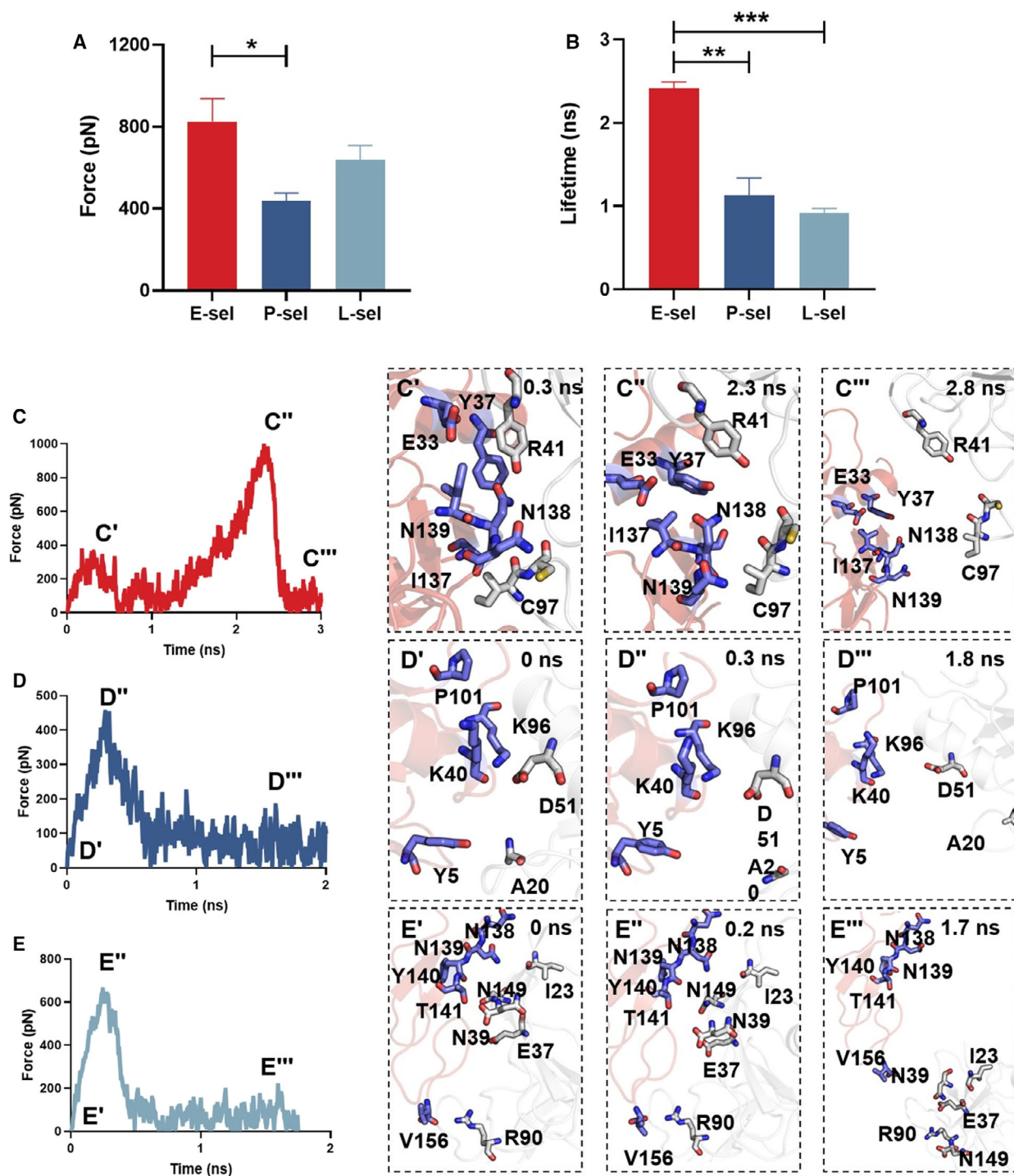


**Fig. 6.** Forced dissociation comparisons among E-/P-/L-selectin-CD44 interactions from SMD simulations. Rupture force (A) and lifetime (B) are presented as the mean  $\pm$  SE of three independent runs with the settings of a pulling velocity of  $5 \text{ nm}\cdot\text{ns}^{-1}$  and a virtual spring constant of  $700 \text{ pN}\cdot\text{nm}^{-1}$ . The pulled and fixed atoms were C-terminal N149- $C_{\alpha}$  of CD44 and C-terminal of selectin EGF domain (V157- $C_{\alpha}$  of E-selectin, D160- $C_{\alpha}$  of P-selectin and V156- $C_{\alpha}$  of L-selectin) respectively, and the force direction was along the vector from the center of I51- $C_{\alpha}$  and C142- $C_{\alpha}$  of selectin to the pulled atom. Typical force curves and corresponding complex conformations around specific moments are shown for E-selectin- (C, C', C'', and C'''), P-selectin- (D, D', D'' and D''') and L-selectin-CD44 (E, E', E'' and E''') interactions, respectively. \* $P < 0.05$ , \*\* $P < 0.01$ , \*\*\* $P < 0.001$ .

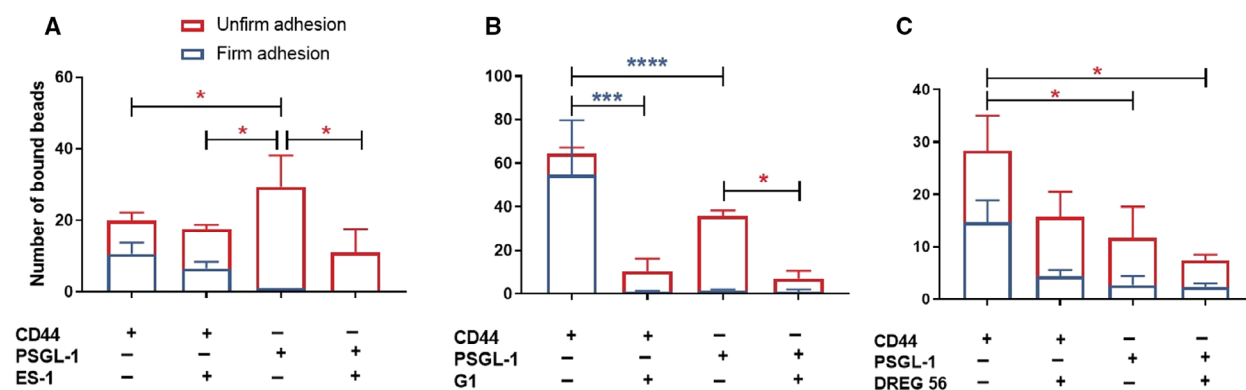


**Fig. 7.** Differences in antibody blocking effect on selectin-CD44 and selectin-PSGL-1 interactions by flow chamber tests. Numbers of both firmly and unfirmly adhered microbeads at the moment of 90s in a time-lapsed course, mediated by selectin-CD44 (left two bars) or selectin-PSGL-1 (right two bars) interactions that were treated without (the first and third bars) or with (the second and fourth bars) blocking antibody, are presented for E-selectin (A) and P-selectin (B) under  $0.5 \text{ dyne}\cdot\text{cm}^{-2}$  and L-selectin under  $1.5 \text{ dyne}\cdot\text{cm}^{-2}$  (C), respectively. Data are shown as the mean  $\pm$  SE of at least three independent repeats. \* $P < 0.05$ , \*\*\* $P < 0.001$ , \*\*\*\* $P < 0.0001$ .

(Fig. S7A,B, first two bars), yielding an insignificant difference in microbead adhesion number, but EDTA chelation significantly decreased the microbead adhesion number mediated by L-selectin-CD44 interactions (Fig. S7C, first two bars). The effects of EDTA chelation on selectin-PSGL-1 interactions were contrary to those for selectin-CD44 interactions (Fig. S7, last two bars). In addition, the adhesion dynamics of microbeads, represented by the distributions of adhesion duration and velocity, exhibited similar trends such that effective blocking by antibodies or EDTA chelation lowered the adhesion duration and enhanced the average velocity of adhered microbeads (Fig. S8). These distinct effects of both antibody blocking and EDTA chelation on selectin-CD44 and selectin-PSGL-1 interactions further supported their different binding sites for selectin, and also validated the predictions of the above molecular docking indirectly.

## Discussion

The variety of isoforms and the complexity of glycosylated modifications of CD44 and differential expression on various types of cells hinder the quantification of selectin-CD44 interactions at the molecular level. Using purified CD44 to avoid the potential uncertainties of CD44 isoforms and glycosylation, the present study systematically compared the interaction differences of three selectin members with respect to their common ligand of CD44 by combining experimental measurements and simulation predictions. Our results indicated that E-selectin-CD44 presents stronger binding and a higher strength than the other two selectins. Meanwhile, selectin-CD44 interactions are different

from selectin-PSGL-1 interactions, presumably attributed to the distinct binding sites of the two ligands with respect to the same selectin member. Quantifying these selectin-CD44 interactions is helpful for understanding their respective contributions to leukocyte migration in the body's immunoreaction, such as the inflammatory response.

Binding kinetics of selectin-CD44 interactions under shear flow were first investigated using a flow chamber assay. Compared with the general analyses of the total number and average rolling velocity of adhered microbeads [21], detailed characteristics, including typical adhesion dynamics patterns, association and dissociation capabilities termed by the number of evolutions of firm adhered microbeads with time, and corresponding shear resistance, were also quantified in the present study. On the one hand, E-selectin-CD44 interactions were confirmed to present the strongest binding compared to the other two members, regardless of the isoforms of purified CD44 or CD44v from LS174T colon carcinoma cells [21]. This finding may correspond to the fact that E-selectin is an intrinsic receptor of CD44 from various types of cell [20–23]. In addition, the most rapid increase of firmly adhered microbeads along time and the similar shear resistance indicated that E-selectin-CD44 interactions have the fastest association and similar dissociation rates under shear stress of  $0.5 \text{ dyne}\cdot\text{cm}^{-2}$  compared to the other two selectin members (Fig. 1). It should be noted that these microbead-based adhesion dynamics were not completely comparable with those of *in vivo* cellular adhesion dynamics as a result of not being in a cellular microenvironment. Indeed, *in vivo* cellular adhesion dynamics are not only determined by receptor-ligand

interactions, but also affected by other factors. Deformable cell carriers would optimize corresponding selectin–ligand interactions [33]. Nano-scale transport or local clustering of a receptor or ligand modulate both the bond formation and dissociation rate dramatically [34–36]. Dynamic subcellular architectures of ‘stepwise peeling of slings’ and ‘pulling of tethers’ and spatial locations of receptor or ligand on these architectures contribute significantly to the cellular adhesion dynamics [37,38]. Although these modulations on CD44–selectin interactions induced by *in vivo* cells could not be replicated using recombinant CD44 and selectins in the present study, the adhesion dynamics of microbeads mediated by CD44 binding to different selectins could also lead to binding differences under comparable experimental conditions. In addition, the limitations of the present study also related to the recombinant CD44-his tag protein only including the HABD domain and the corresponding glycosylated modifications. The contributions of the stem domain or variant parts of CD44 to CD44–selectin interactions were not clear because those constructs were not commercially available. Furthermore, the direct physisorption of the CD44 ligand on the substrate in the flow chamber assay was not able to exclude the effect of the randomness of molecular orientations, which is distinct from *in vivo* constitutive expression, also affecting CD44–selectin interaction mediated microbead adhesions. In brief, although the qualitative trends among three selectin members were consistent with those of CD44v from LS174T colon carcinoma cells or the standard isoform of CD44 (CD44s) on hematopoietic-progenitor cells or on HL-60 cells [21], the quantitative features of CD44–selectin interactions and the corresponding cellular adhesion dynamics need to be quantified further under *in vivo* conditions.

On the other hand, the L-selectin–CD44 interaction showed an exceptional enhancement with more adhered microbeads under shear stress of  $1.5 \text{ dyne}\cdot\text{cm}^{-2}$  compared to that of  $0.5 \text{ dyne}\cdot\text{cm}^{-2}$ , although the other two selectin members showed conventional decreases of adhered microbeads with increased shear stress. This shear stress-induced strengthening of L-selectin–CD44 interactions was similar to the shear stress-enhanced T-cell and neutrophil adhesion on CD44 that is expressed in the KG1a layer under a specific shear stress range [39], but was contrary to the monotonic decreases of L-selectin–CD44v interactions with an increase of shear stress [21]. Indeed, P-selectin–CD44 interaction-mediated aggregation between platelets and LS174T cells also demonstrated the shear stress-induced enhancement [40]. These results indicated the tight dependence of selectin–CD44 interactions on shear stress, which appears to be

reasonable because *in vivo* physiological blood flow is a key regulation factor. The exceptional enhancement of CD44–L-selectin interactions from a shear stress of  $0.5\text{--}1.5 \text{ dyne}\cdot\text{cm}^{-2}$  implied a possible catch-bond mechanism, such as those of selectin–PSGL-1 interactions [6,12,13,15,16]. Evidently, the elaborative mechanisms of shear stress on selectin–CD44 interactions and the corresponding differences among three selectin members require future investigation.

Integrated comparisons of different selectin–CD44 interaction strengths were conducted using an AFM assay for the first time. Again, the E-selectin–CD44 system exhibited the strongest interactions with the largest rupture forces, regardless of any variation of contact time and retract velocity. The mechanical strength of the L-selectin–CD44 system was higher than that of the P-selectin–CD44 system with a short contact time of 50 ms, but the two systems became almost comparable with a long contact time of 500 ms, implying that the P-selectin–CD44 system requires a longer time to form a stable molecular bond. The rupture force of the P-selectin–CD44 pair measured here was comparable to that of P-selectin binding to CD44v immunoprecipitated from LS174T cell lysates reported previously, even under the smaller loading rate range [27]. Moreover, both rupture forces and zero-force Bell model parameters do not change much with different contact times of 2, 20 and 200 ms for P-selectin–CD44v interactions [27], but the selectin–CD44 interactions in the present study all showed an increased rupture force and  $k_r^0$  and a decreased reactive compliance when the contact time increased from 50 to 500 ms. These differences may result from the differences in the CD44 isoforms or the functionalized protocol in the AFM experiments.

Perhaps the most interesting finding from the present study was the microstructural predictions of the selectin–CD44 interaction using both molecular docking and MD simulations. On the one hand, combination of the binding free energy analysis in equilibration simulations with the estimation of rupture forces and lifetimes in *ev*-SMD simulations further confirmed that the E-selectin–CD44 interactions presented the strongest binding. On the other hand, the different binding epitopes among the three selectin members to their common ligand of CD44 indicated the diversity and sensitivity of selectin–CD44 interactions. This was distinct from that of the selectin–PSGL-1 interactions, for which PSGL-1 is considered to bind to similar epitopes of selectins [2]. Furthermore, the binding epitopes of selectin–CD44 interactions predicted in the present study were entirely different from those of selectin–PSGL-1 interactions. The binding sites of the former mainly locate at the sides of the axis linking the

centers of the lectin and EGF domains, whereas those of the latter locate at the head face of the lectin domain, including the calcium ion that is perpendicular to the axis [2]. These differences may explain the rapid association rate of selectin–PSGL-1 interactions required for mediating the effective capture of leukocytes from blood flow and the following rapid rolling along the endothelium, in that the binding between calcium ion and FUC glucoside dominated in selectin–PSGL-1 interactions is certainly faster than other types of non-bond interactions. In addition, the distinct binding epitopes of PSGL-1 and CD44 to selectins also offered a potential cooperation between the two selectin ligands through binding to a same selectin molecule, as seen in their colocations on leukocytes [41]. It should be noted that consideration of the effect of glycosylation was beyond the scope of the present as a result of missing glycosylations in the crystallized CD44 HABD domain.

Collectively, the present study compared the capabilities among the interactions of three selectin members with CD44 with respect to mediating cellular adhesions under shear flow, quantified their mechanical strengths and explored the corresponding microstructural mechanisms. Our results offer basic data for understanding the functional differences among the E-, P- and L-selectins with respect to CD44 ligand, as well as the differences between the two ligands of PSGL-1 and CD44.

## Materials and methods

### Reagents

PE-labeled anti-human CD62E (336008)/CD62P (304906)/CD62L (304806) antibodies and isotype-matched mouse IgG1 $\kappa$  (400112) were obtained from BioLegend (San Diego, CA, USA). Recombinant human E-Selectin/CD62E (724-ES-100), P-Selectin/CD62P (137-PS-050) and L-Selectin/CD62L (728-LS-100) Fc chimeras were purchased from R&D Systems (Minneapolis, MN, USA). Recombinant human CD44-his tag protein (12211-H08H) and PSGL-1-his tag protein (13863-H08H) were purchased from Sino Biological (Beijing, China). Goat anti-human IgG H&L (Biotin) (ab6857) was purchased from Abcam (Cambridge, MA, USA). Anti-human IgG (Fc specific) (I2136) was purchased from Sigma-Aldrich (St Louis, MO, USA). Anti-E-selectin and -P-selectin antibodies ES-1 and G1 as a gift were from R. P. McEver at Oklahoma Medical Research Foundation (Oklahoma, OK, USA) and anti-L-selectin antibody DREG 56 (ab254540) was purchased from Abcam. EDTA (17892) was obtained from Thermo Fisher Scientific (Waltham, MA, USA). Streptavidin-coated silica microspheres were obtained from Bangs Laboratories, Inc.

(Fishers, IN, USA). Dulbecco's phosphate-buffered saline (DPBS; SH30028.02) and Hank's balanced salt solution (SH30268.01) were purchased from Hyclone (Logan, UT, USA).

### Parallel-plate flow chamber assay

A flow chamber (length 2 cm, width 0.5 cm, height 0.01 inch) was assembled using a circular flow cell system (#31-001; GlycoTech, Gaithersburg, MD, USA) and used to quantify the binding dynamics of E-, P- and L-selectins to their common ligands of CD44 or PSGL-1. Ligands of CD44 (10  $\mu\text{g}\cdot\text{mL}^{-1}$ ) or PSGL-1 (10  $\mu\text{g}\cdot\text{mL}^{-1}$ ) were directly coated on a sterile 35-mm tissue culture dish by physical absorption. Briefly, 10  $\mu\text{L}$  of CD44 or 10  $\mu\text{L}$  of PSGL-1 was incubated on an area of  $0.5 \times 0.5$  cm for 2 h at 37 °C. The coating area was then washed three times using DPBS followed by blocking the incubation of 1% BSA for 2 h at 37 °C. Separately, flowing microbeads were coated with E-/P-/L-selectin-Fc constructs at a final concentration of  $10^5$   $\text{mL}^{-1}$ . Here, 100  $\mu\text{L}$  of streptavidin-modified silica microbeads of approximately 5  $\mu\text{m}$  in diameter in 400  $\mu\text{L}$  of DPBS dilution were incubated with 2  $\mu\text{L}$  (2  $\text{mg}\cdot\text{mL}^{-1}$ ) of biotin-conjugated goat-anti-human IgG-Fc antibody and shaken for 4 h. After washing three times in DPBS, 20  $\mu\text{L}$  (100  $\mu\text{g}\cdot\text{mL}^{-1}$ ) of E-, P-, or L-selectin-Fc was added to 500  $\mu\text{L}$  of prepared solution for 12 h at 4 °C with shaking at 180 r.p.m. After washing three times in DPBS followed by blocking with 1% BSA for 2 h at 37 °C, the collected microbeads were ready for the flow chamber assay. Microbeads without a selectin coating served as the blank control (Fig. S1A).

Each flow chamber test included two sequential processes (Fig. S1B). The first was designed to investigate selectin–CD44 binding capability by continuously filling the microbead suspension under a constant shear stress of 0.5 or 1.5  $\text{dyne}\cdot\text{cm}^{-2}$  for 210 s. The second was performed just after the first process, switching the microbead suspension to blank Hank's balanced salt solution, with stepwise increased shear stress from 1 to 48  $\text{dyne}\cdot\text{cm}^{-2}$  for 30 s each, to quantify the shear-resistance of selectin–CD44 interactions. The tests for elucidating the effects of EDTA chelation or antibody blocking on selectin–ligand interactions were conducted by filling with EDTA solution or blocking antibody pre-incubated microbead suspension in the first process. The binding capability of selectin–ligand interactions was characterized by the numbers of firmly or unfirmly adhered microbeads, the average velocity and the duration distributions of adhered microbeads. Here, microbeads were defined as having a firm adhesion if they remained motionless for at least 5 s, and other microbeads involved in instantaneous or short-lived adhesions under shear stress were denoted as having an unfirm adhesion with a velocity in the range 0–70  $\mu\text{m}\cdot\text{s}^{-1}$ . Data for average velocity and duration distributions of adhered microbeads were based on a typical time window of 5 s around the

moment of 90 s. The shear-resistance of selectin–ligand interactions was represented by the evolution of the normalized microbead numbers remaining adhered at the 30-s moment of each stress.

### Flow cytometry

A flow cytometry assay was used to test the coating density of selectins on microbeads. In brief, 100  $\mu\text{L}$  of selectin-coated microbead suspensions, as described above, were incubated with PE-conjugated anti-selectin mAbs (5  $\mu\text{L}$ ) for 30 min on ice, and then resuspended into 400  $\mu\text{L}$  of DPBS. After washing three times, the microbeads were analyzed by flow cytometry (BD Biosciences, San Jose, CA, USA). PE-labeled mouse IgG1 $\kappa$  isotypes were used as the control (Fig. S1C). The coating densities of E-, P- and L-selectins were comparable for the subsequent flow chamber tests that aimed to quantify their binding differences to common ligands of CD44 or PSGL-1 (Fig. S1D).

### AFM assay

A Bioscope MultiMode8 AFM (Bruker, Billerica, MA, USA) was used to determine the mechanical strength of selectin–CD44 interactions. Commercial cantilevers of MLCT (Veeco; Bruker) were used with a nominal spring constant  $k_c$  of 10 pN·nm<sup>-1</sup> (cantilever C). The cantilevers were functionalized with CD44 by direct physical absorption. Briefly, the cantilevers were first incubated in a 100  $\mu\text{g}\cdot\text{mL}^{-1}$  solution of CD44 for 2 h at 37 °C and, after washing three times in DPBS, they were blocked in 1% BSA for 2 h at 37 °C until use. The substrates were functionalized with different selectins via capture of anti-Fc antibodies. In brief, anti-Fc antibody (2 mg·mL<sup>-1</sup>) was physically absorbed to a fresh mica for 2 h at 37 °C, and then selectins (10  $\mu\text{g}\cdot\text{mL}^{-1}$ ) were incubated on the mica surface for 2 h at 37 °C. Finally, the mica substrate was blocked with 1% BSA for 2 h at 37 °C. The substrates without selectin capture were used for the control (Fig. S4A).

The selectin functionalized mica was placed on the AFM stage, which was repeatedly driven to approach the CD44-coated cantilever tip, to make contact at a compressive force allowing reversible bond formation and dissociation, and to retract away allowing observation of the adhesion event and measurement of rupture force, if any. The adhesion and force signals for each approach–contact–retract cycle were collected by a quad photodetector (Fig. S4A). The approach velocity and compressive force were set as 1  $\mu\text{m}\cdot\text{s}^{-1}$  and 150 pN for all experiments, respectively. The contact time between the cantilever and mica was set as 50 or 500 ms, and five different retract velocities of 0.5, 1, 2, 4 and 8  $\mu\text{m}\cdot\text{s}^{-1}$  were set for each selectin–CD44 system. Each cantilever was calibrated by thermal tune method (calculated upon the deflection sensitivity values ranging between 180 and 200 nm·V<sup>-1</sup>) before the experiments. Different

locations on each mica were tested for 100 cycles at each location. All experiments were independently repeated at least three times, and at least 200 adhesion events and rupture forces were obtained in each case. Low molecular densities were used to control infrequent binding (< 35%). In addition to the measured adhesion frequency and rupture force, systematic spring constant  $k$  was also collected for demonstrating the distinct interactions of the three selectin members to CD44 ligand (Fig. S4B).

DFS theory was used to predict binding kinetics based on the relationship between rupture forces and loading rates. It is assumed that the selectin–CD44 bond follows the first-order irreversible dissociation kinetics. The reverse rate,  $k_r$ , is assumed to be an exponential function of applied force,  $f$ , as Eqn (1) [42]:

$$k_r(f) = k_r^0 \exp\left(\frac{af}{k_B T}\right) \quad (1)$$

where  $k_B$  is the Boltzmann constant,  $T$  is the absolute temperature and  $a$  is the so-called reactive compliance representing the width of the energy well that kinetically traps the interacting molecules in the bound state. Assuming that the reverse rate  $k_r$  depends on time  $t$  through the force  $f$ , which is equal to the loading rate  $r_f$  (retract velocity  $\times$  spring constant) times  $t$ , it follows that the most probable rupture force or peak force,  $f_m$ , vs  $\ln(r_f)$  should be a straight line as Eqn (2) [43]:

$$f_m = \frac{k_B T}{a} \ln(r_f) - \frac{k_B T}{a} \ln\left(\frac{k_r^0 k_B T}{a}\right). \quad (2)$$

Thus zero-force reverse rate  $k_r^0$  and reactive compliance  $a$  can be obtained by fitting the data to Eqn (2).

### Molecular docking

Molecular docking was used to predict selectin–CD44 binding sites. Corresponding structures for docking were extracted from the Protein Data Bank ([www.pdb.rcsb.org](http://www.pdb.rcsb.org)) including E-/P-/L-selectin lectin and EGF domains with the respective PDB codes of 1G1T [2], 1G1Q [2] and 3CFW [44] and CD44 HABD domain with a PDB code of 1UUH [29]. The DOCKING software of AUTODOCK, version 4.2 was used with a ‘rigid’ docking strategy for both selectin receptor and CD44 ligand [45]. Grid maps were created at the geometric center of the selectin receptor including the Ca<sup>2+</sup> ion and set as sufficiently large to enclose > 70% of amino acids of the target selectin with spacing of 0.375 Å for effective searching by CD44 ligand. A Lamarckian genetic algorithm was used to perform the searching and to calculate the binding free energy of the potential selectin–CD44 complex at each searching site, and the maximum number of searching sites and corresponding energy evaluations was set as 2 500 000. Other related parameters were set as default values. Finally, 50 optimal complex candidates

based on binding free energy were chosen for further binding site analyses for each selectin–CD44 system.

### Molecular dynamics simulations

To evaluate the binding differences of three selectins to CD44, MD simulations were further performed based on the optimal selectin–CD44 complex with the lowest binding free energy resulting from docking outputs. Each simulation system was built by solvating the target selectin–CD44 complex into a rectangular water box and neutralizing with approximately 150 mM Na<sup>+</sup> and Cl<sup>−</sup> ions to mimic the physiological ionic concentration. MD simulations were carried out using NAMD [46] with the all-atom force field of CHARMM27 [47]. Prior to the equilibration process, energy minimization was initiated with 100 000 steps by fixing I51-C<sub>α</sub> of selectin. System heating was then performed from 0 to 310 K at increments of 10 K every 1 ps. At last two independent runs of 50-ns free equilibrations were performed under the grand canonical ensemble of NPT for each selectin–CD44 system. An integration time step of 1 fs and the periodic boundary conditions were applied in the MD simulations. A smooth (10–14 Å) cut-off and the Particle Mesh Ewald method were employed to calculate van der Waals forces and full electrostatics, respectively. The heat bath at 310 K was manipulated under a Langevin thermostat, and the pressure at 1 atm was controlled by the Nosé–Hoover Langevin piston method. SMD simulations were also conducted to test the mechanical strength of the selectin–CD44 complex. Here, each complex was forced to dissociate using constant velocity SMD (cv-SMD), where the C-terminal atom N149-C<sub>α</sub> of CD44 ligand was pulled via a virtual spring with a spring constant of 700 pN·nm<sup>−1</sup> at a constant speed of 5 nm·ns<sup>−1</sup> along the vector from the centers of I51-C<sub>α</sub> and C142-C<sub>α</sub> to the pulled end. The C-terminal of selectin EGF domain was fixed (V157-C<sub>α</sub> of E-selectin, D160-C<sub>α</sub> of P-selectin and V156-C<sub>α</sub> of L-selectin).

Analyses of MD simulations included the non-bonded interaction and pairwise free energy of each selectin–CD44 complex, using the molecular mechanics Poisson–Boltzmann surface area module of AMBERTOOLS18 [48] and based on the generalized Born model [49]. Rupture forces and lifetimes based on SMD simulations were also compared among the three selectin–CD44 complexes. All system construction and structural analyses were performed using VMD [50]. PYMOL was used for visualization.

### Acknowledgements

MD simulations were performed on the National Supercomputer Center in Tianjin. This work was supported by National Key Research and Development Program of China grant 2016YFA0501601, National Natural Science Foundation of China grant 11972042, Frontier Science Key Project of Chinese Science

Academy grant QYZDJ-SSW-JSC018 and Strategic Priority Research Program of Chinese Academy of Sciences grant XDB22040101. All institutional and national guidelines for the care and use of laboratory animals were followed.

### Conflicts of interest

The authors declare no conflict of interest.

### Author contributions

LL performed the flow chamber experiments, analyzed the data and prepared the figures. QD performed the AFM experiments, the docking and MD simulations, analyzed the data, and prepared the figures. JZ analyzed the AFM data. YW prepared the figures. MZ analyzed the MD simulations. XG interpreted the data and revised the paper. ML designed the study, analyzed and interpreted the data, and revised the paper. SL designed the study, analyzed and interpreted the data, drafted the article, and approved the final version of the article for publication. All authors reviewed the results and approved the final version of the manuscript submitted for publication.

### Peer review

The peer review history for this article is available at <https://publons.com/publon/10.1111/febs.16303>.

### Data availability statement

All data generated or analyzed in this study are included in the figures and the supplementary material of this article.

### References

- McEver RP (2002) Selectins: lectins that initiate cell adhesion under flow. *Curr Opin Cell Biol* **14**, 581–586.
- Somers WS, Tang J, Shaw GD & Camphausen RT (2000) Insights into the molecular basis of leukocyte tethering and rolling revealed by structures of P- and E-selectin bound to SLe(X) and PSGL-1. *Cell* **103**, 467–479.
- Lü SQ & Long M (2005) Forced dissociation of selectin–ligand complexes using steered molecular dynamics simulation. *Mol Cell Biomech* **2**, 161–177.
- Lü SQ, Zhang Y & Long M (2010) Visualization of allostery in P-selectin lectin domain using MD simulations. *PLoS One* **5**, e15417.
- Lü SQ, Chen S, Mao DB, Zhang Y & Long M (2015) Contribution of the CR domain to P-selectin lectin

- domain allostery by regulating the orientation of the EGF domain. *PLoS One* **10**, e0118083.
- 6 Lou J & Zhu C (2007) A structure-based sliding-rebinding mechanism for catch bonds. *Biophys J* **92**, 1471–1485.
  - 7 Springer TA (2009) Structural basis for selectin mechanochemistry. *Proc Natl Acad Sci USA* **106**, 91–96.
  - 8 Huang J, Chen J, Chesla SE, Yago T, Mehta P, McEver RP, Zhu C & Long M (2004) Quantifying the effects of molecular orientation and length on two-dimensional receptor-ligand binding kinetics. *J Biol Chem* **279**, 44915–44923.
  - 9 Wu L, Xiao B, Jia X, Zhang Y, Lü SQ, Chen J & Long M (2007) Impact of carrier stiffness and microtopology on two-dimensional kinetics of P-selectin and P-selectin glycoprotein ligand-1 (PSGL-1) interactions. *J Biol Chem* **282**, 9846–9854.
  - 10 Sun GY, Zhang Y, Huo B & Long M (2009) Surface-bound selectin-ligand binding is regulated by carrier diffusion. *Eur Biophys J* **38**, 701–711.
  - 11 Lü SQ, Ye ZY, Zhu C & Long M (2006) Quantifying the effects of contact duration, loading rate, and approach velocity on P-selectin-PSGL-1 interactions using AFM. *Polymer* **47**, 2539–2547.
  - 12 Marshall BT, Long M, Piper JW, Yago T, McEver RP & Zhu C (2003) Direct observation of catch bonds involving cell-adhesion molecules. *Nature* **423**, 190–193.
  - 13 Lou J, Yago T, Klopocki AG, Mehta P, Chen W, Zarnitsyna VI, Bovin NV, Zhu C & McEver RP (2006) Flow-enhanced adhesion regulated by a selectin interdomain hinge. *J Cell Biol* **174**, 1107–1117.
  - 14 Puri KD, Finger EB & Springer TA (1997) The faster kinetics of L-selectin than of E-selectin and P-selectin rolling at comparable binding strength. *J Immunol* **158**, 405–413.
  - 15 Zhu C (2014) Mechanochemistry: a molecular biomechanics view of mechanosensing. *Ann Biomed Eng* **42**, 388–404.
  - 16 Zhu C, Yago T, Lou J, Zarnitsyna VI & McEver RP (2008) Mechanisms for flow-enhanced cell adhesion. *Ann Biomed Eng* **36**, 604–621.
  - 17 Yago T, Shao B, Miner JJ, Yao L, Klopocki AG, Maeda K, Coggeshall KM & McEver RP (2010) E-selectin engages PSGL-1 and CD44 through a common signaling pathway to induce integrin  $\alpha$ L $\beta$ 2-mediated slow leukocyte rolling. *Blood* **116**, 485–494.
  - 18 Gong YX, Zhang Y, Feng S, Liu X, Lü SQ & Long M (2017) Dynamic contributions of P- and E-selectins to  $\beta$ 2-integrin-induced neutrophil transmigration. *FASEB J* **31**, 212–223.
  - 19 Huang D, Ding Q, Chen S, Lü SQ, Zhang Y & Long M (2021) E-selectin negatively regulates polymorphonuclear neutrophil transmigration through altered endothelial junction integrity. *FASEB J* **35**, e21521.
  - 20 Hidalgo A, Peired AJ, Wild M, Vestweber D & Frenette PS (2007) Complete identification of E-selectin ligands on neutrophils reveals distinct functions of PSGL-1, ESL-1, and CD44. *Immunity* **26**, 477–489.
  - 21 Hanley WD, Napier SL, Burdick MM, Schnaar RL, Sackstein R & Konstantopoulos K (2006) Variant isoforms of CD44 are P- and L-selectin ligands on colon carcinoma cells. *FASEB J* **20**, 337–339.
  - 22 Hanley WD, Burdick MM, Konstantopoulos K & Sackstein R (2005) CD44 on LS174T colon carcinoma cells possesses E-selectin ligand activity. *Cancer Res* **65**, 5812–5817.
  - 23 Nacher M, Blazquez AB, Shao B, Matesanz A, Prophete C, Berin MC, Frenette PS & Hidalgo A (2011) Physiological contribution of CD44 as a ligand for E-selectin during inflammatory T-cell recruitment. *Am J Pathol* **178**, 2437–2446.
  - 24 Ali AJ, Abuelela AF & Merzaban JS (2017) An analysis of trafficking receptors show that CD44 and P-selectin glycoprotein ligand-1 collectively control the migration of activated human T-cells. *Front Immunol* **8**, 492.
  - 25 AbuSamra DB, Al-Kilani A, Hamdan SM, Sakashita K, Gadhoum SZ & Merzaban JS (2015) Quantitative characterization of E-selectin Interaction with native CD44 and P-selectin Glycoprotein Ligand-1 (PSGL-1) using a real time immunoprecipitation-based binding assay. *J Biol Chem* **290**, 21213–21230.
  - 26 AbuSamra DB, Aleisa FA, Al-Amoodi AS, Ahmed HMJ, Chin CJ, Abuelela AF, Bergam P, Sougrat R & Merzaban JS (2017) Not just a marker: CD34 on human hematopoietic stem/progenitor cells dominates vascular selectin binding along with CD44. *Blood Adv* **1**, 2799–2816.
  - 27 Raman PS, Alves CS, Wirtz D & Konstantopoulos K (2011) Single-molecule binding of CD44 to fibrin versus P-selectin predicts their distinct shear-dependent interactions in cancer. *J Cell Sci* **124**, 1903–1910.
  - 28 Naor D, Sionov RV & Ish-Shalom D (1997) CD44: structure, function, and association with the malignant process. *Adv Cancer Res* **71**, 241–319.
  - 29 Teriete P, Banerji S, Noble M, Blundell CD, Wright AJ, Pickford AR, Lowe E, Mahoney DJ, Tammi MI, Kahmann JD et al. (2004) Structure of the regulatory hyaluronan binding domain in the inflammatory leukocyte homing receptor CD44. *Mol Cell* **13**, 483–496.
  - 30 Takeda M, Ogino S, Umemoto R, Sakakura M, Kajiwara M, Sugahara KN, Hayasaka H, Miyasaka M, Terasawa H & Shimada I (2006) Ligand-induced structural changes of the CD44 hyaluronan-binding domain revealed by NMR. *J Biol Chem* **281**, 40089–40095.
  - 31 Banerji S, Wright AJ, Noble M, Mahoney DJ, Campbell ID, Day AJ & Jackson DG (2007) Structures



- of the Cd44-hyaluronan complex provide insight into a fundamental carbohydrate-protein interaction. *Nat Struct Mol Biol* **14**, 234–239.
- 32 Vuorio J, Vattulainen I & Martinez-Seara H (2017) Atomistic fingerprint of hyaluronan-CD44 binding. *PLoS Comput Biol* **13**, e1005663.
- 33 Yago T, Leppanen A, Qiu H, Marcus WD, Nollert MU, Zhu C, Cummings RD & McEver RP (2002) Distinct molecular and cellular contributions to stabilizing selectin-mediated rolling under flow. *J Cell Biol* **158**, 787–799.
- 34 Gopalakrishnan M, Forsten-Williams K, Nugent MA & Tauber UC (2005) Effects of receptor clustering on ligand dissociation kinetics: theory and simulations. *Biophys J* **89**, 3686–3700.
- 35 Schmidt BJ, Papin JA & Lawrence MB (2009) Nanomotion dynamics are determined by surface-tethered selectin mechanokinetics and bond formation. *PLoS Comput Biol* **5**, e1000612.
- 36 AbuZineh K, Joudeh LI, Al Alwan B, Hamdan SM, Merzaban JS & Habuchi S (2018) Microfluidics-based super-resolution microscopy enables nanoscopic characterization of blood stem cell rolling. *Sci Adv* **4**, eaat5304.
- 37 Sundd P, Gutierrez E, Koltsova EK, Kuwano Y, Fukuda S, Pospieszalska MK, Groisman A & Ley K (2012) 'Slings' enable neutrophil rolling at high shear. *Nature* **488**, 399–403.
- 38 Al Alwan B, AbuZineh K, Nozue S, Rakhmatulina A, Aldehaiman M, Al-Amoodi AS, Serag MF, Aleisa FA, Merzaban JS & Habuchi S (2021) Single-molecule imaging and microfluidic platform reveal molecular mechanisms of leukemic cell rolling. *Commun Biol* **4**, 868.
- 39 Dimitroff CJ, Lee JY, Schor KS, Sandmaier BM & Sackstein R (2001) Differential L-selectin binding activities of human hematopoietic cell L-selectin ligands, HCELL and PSGL-1. *J Biol Chem* **276**, 47623–47631.
- 40 Alves CS, Burdick MM, Thomas SN, Pawar P & Konstantopoulos K (2008) The dual role of CD44 as a functional P-selectin ligand and fibrin receptor in colon carcinoma cell adhesion. *Am J Physiol-Cell Physiol* **294**, C907–C916.
- 41 Erhani J, Tay J, Barbier V, Levesque JP & Winkler IG (2020) Acute myeloid leukemia chemo-resistance is mediated by E-selectin receptor CD162 in bone marrow niches. *Front Cell Dev Biol* **8**, 668.
- 42 Bell GI (1978) Models for the specific adhesion of cells to cells. *Science* **200**, 618–627.
- 43 Evans E & Ritchie K (1997) Dynamic strength of molecular adhesion bonds. *Biophys J* **72**, 1541–1555.
- 44 Mehta-D'souza P, Klopocki AG, Oganessian V, Terzyan S, Mather T, Li Z, Panicker SR, Zhu C & McEver RP (2017) Glycan bound to the selectin low affinity state engages Glu-88 to stabilize the high affinity state under force. *J Biol Chem* **292**, 2510–2518.
- 45 Morris GM, Huey R, Lindstrom W, Sanner MF, Belew RK, Goodsell DS & Olson AJ (2009) AutoDock4 and AutoDockTools4: automated docking with selective receptor flexibility. *J Comput Chem* **30**, 2785–2791.
- 46 Phillips JC, Braun R, Wang W, Gumbart J, Tajkhorshid E, Villa E, Chipot C, Skeel RD, Kale L & Schulten K (2005) Scalable molecular dynamics with NAMD. *J Comput Chem* **26**, 1781–1802.
- 47 MacKerell AD, Bashford D, Bellott M, Dunbrack RL, Evanseck JD, Field MJ, Fischer S, Gao J, Guo H, Ha S *et al.* (1998) All-atom empirical potential for molecular modeling and dynamics studies of proteins. *J Phys Chem B* **102**, 3586–3616.
- 48 Case DA, Cheatham TE, Darden T, Gohlke H, Luo R, Merz KM Jr, Onufriev A, Simmerling C, Wang B & Woods RJ (2005) The Amber biomolecular simulation programs. *J Comput Chem* **26**, 1668–1688.
- 49 Lee MC, Yang R & Duan Y (2005) Comparison between Generalized-Born and Poisson-Boltzmann methods in physics-based scoring functions for protein structure prediction. *J Mol Model* **12**, 101–110.
- 50 Humphrey W, Dalke A & Schulten K (1996) VMD: visual molecular dynamics. *J Mol Graph* **14**, 33–38.

## Supporting information

Additional supporting information may be found online in the Supporting Information section at the end of the article.

**Fig. S1.** Schematic of the flow chamber set-up.

**Fig. S2.** Comparisons of adhesion dynamics of microbeads mediated by E-/P-/L-selectin-CD44 interactions under shear stress of 0.5 dyne·cm<sup>-2</sup>.

**Fig. S3.** Differences in E-/P-/L-selectin-CD44 interactions under shear stress of 1.5 dyne·cm<sup>-2</sup>.

**Fig. S4.** Schematic of the AFM tests.

**Fig. S5.** Molecular docking between E-/P-/L-selectin-CD44 interactions.

**Fig. S6.** Comparisons of adhesion dynamics of microbeads mediated by PSGL-1 binding to E-/P-selectin under shear stress of 0.5 dyne·cm<sup>-2</sup> and to L-selectin of 1.5 dyne·cm<sup>-2</sup>.

**Fig. S7.** Effects of EDTA chelation on microbead adhesions mediated by E-/P-/L-selectin-CD44 or PSGL-1 interactions.

**Fig. S8.** Effects of EDTA chelation and antibody blocking on microbead adhesion dynamics mediated by E-/P-/L-selectin-CD44 or -PSGL-1 interactions.

**Video S1.** Adhesion dynamics of microbeads mediated by a specific E-selectin–CD44 interaction under shear stress of  $0.5 \text{ dyne}\cdot\text{cm}^{-2}$ .

**Video S2.** Adhesion dynamics of microbeads mediated by a specific P-selectin–CD44 interaction under shear stress of  $0.5 \text{ dyne}\cdot\text{cm}^{-2}$ .

**Video S3.** Adhesion dynamics of microbeads mediated by a specific L-selectin–CD44 interaction under shear stress of  $0.5 \text{ dyne}\cdot\text{cm}^{-2}$ .

**Video S4.** Adhesion dynamics of microbeads mediated by a non-specific interaction between Bio-anti-Fc antibody and CD44 under shear stress of  $0.5 \text{ dyne}\cdot\text{cm}^{-2}$ .